AGU PUBLICATIONS

Paleoceanography

RESEARCH ARTICLE
10.1002/2015PA002904

Key Points:
- Oxygen minimum zone intensity in Gulf of California during late Holocene interpreted from $\delta^{15}N_{sed}$
- Late Holocene is characterized by rapid OMZ intensification followed by more gradual reoxygenation
- OMZ strength and organic carbon productivity/export related to Pacific Decadal Oscillation and solar cycles

Supporting Information:
- Supporting Information S1

Correspondence to:
C. E. Tems,
tems@usc.edu;
caitlin.tems@gcccd.edu

Citation:
Tems, C. E., W. M. Berelson, R. Thunell, E. Tappa, X. Xu, D. Khider, S. Lund, O. González-Yajimovich, and Y. Hamann (2016), Decadal to centennial fluctuations in the intensity of the eastern tropical North Pacific oxygen minimum zone during the last 1200 years, *Paleoceanography*, *31*, 1138–1151, doi:10.1002/2015PA002904.

Received 18 NOV 2015
Accepted 22 JUL 2016
Accepted article online 26 JUL 2016
Published online 31 AUG 2016

Decadal to centennial fluctuations in the intensity of the eastern tropical North Pacific oxygen minimum zone during the last 1200 years

Caitlin E. Tems[1], William M. Berelson[1], Robert Thunell[2], Eric Tappa[2], Xiaomei Xu[3], Deborah Khider[1], Steve Lund[1], Oscar González-Yajimovich[4], and Yvonne Hamann[5]

[1]Department of Earth Sciences, University of Southern California, Los Angeles, California, USA, [2]School of the Earth, Ocean and Environment, University of South Carolina, Columbia, South Carolina, USA, [3]Department of Earth System Science, University of California, Irvine, California, USA, [4]Facultad de Ciencias Marinas, Universidad Autonoma de Baja California, Ensenada, Mexico, [5]Institute of Biogeochemistry and Pollutant Dynamics, Eidgenössische Technische Hochschule, Zurich, Switzerland

Abstract Oxygen minimum zones (OMZs), located below highly productive marine regions, are sites of microbially mediated denitrification and biogeochemical cycling that have global significance. The intensity of OMZs fluctuates naturally; however, the degree of these fluctuations and a comprehensive understanding of the factors that drive these fluctuations on decadal to centennial time scales is lacking. Our high-resolution (near-annual) record of $\delta^{15}N_{sed}$ from laminated sediments at the Pescadero Slope in the Gulf of California (eastern tropical North Pacific) fluctuates between maximum values of 10.5‰ and minimum values of 8.0‰ over the past 1200 years. An analysis of the relationship between $\delta^{15}NO_3^-$ and $[O_2]$ in the water column suggests that the observed range of $\delta^{15}N_{sed}$ values is equivalent to an approximately 8 μM fluctuation in O_2 content and that these changes can occur in less than 25 years. Our findings show that the OMZ typically intensifies quickly and contracts gradually; the average rate of OMZ intensification ($-0.24\ \mu M\ O_2$/yr) is twice as fast as the rate of OMZ reoxygenation. Spectral analyses of the $\delta^{15}N_{sed}$ record and Br/Cl counts, with the latter are used as a proxy for organic carbon preservation, suggest that the Pacific Decadal Oscillation and the Suess (deVries) solar cycle (solar irradiance) may influence the intensity of the OMZ and carbon production/export during the late Holocene. Coherence between $\delta^{15}N_{sed}$ and weight percent organic carbon also suggests that similar mechanisms influence both OMZ fluctuations and variation in organic carbon production/export.

1. Introduction

Oceanic oxygen minimum zones (OMZs) are midwater features that are associated with expansive, highly productive regions of the ocean and are also sites of microbially mediated biogeochemical cycling of redox sensitive compounds [*Gilly et al*., 2013; *Keeling et al*., 2010]. These regions have important implications for nitrogen loss (through denitrification and anammox), ecological relationships, marine economic recourses, and ocean management since the world's most productive fisheries are found above OMZs. Variations in dissolved oxygen concentrations $[O_2]$ and OMZ intensity are hypothesized to have triggered the end-Permian mass extinction [*Benton and Twitchett*, 2003; *Wingall and Twitchett*, 1996] and the great ocean anoxia events in the Cretaceous period [*Jones and Jenkyns*, 2001], which had devastating impacts on marine communities and changed the cycling of nutrients and trace metals on regional and global scales. The magnitude and intensity of OMZs have been shown to vary on glacial-interglacial time scales [*Altabet et al*., 1995; *Ganeshram et al*., 2000; *Deutsch et al*., 2004; *Thunell and Kepple*, 2004], suggesting a relationship between the climate system and the expanse of OMZs. Additionally, Millennial $\delta^{15}N_{sed}$ records have been reconstructed in the eastern tropical South Pacific (ETSP) and suggest that ETSP OMZ intensity could be influenced by latitudinal shifts in the Intertropical Convergence Zone (ITCZ) [*Agnihotri et al*., 2008; *Gutiérrez et al*., 1997; *Chazen et al*., 2009]. In this study we generate high-resolution records for the eastern tropical North Pacific (ETNP), which are used to investigate and compare mechanisms influencing denitrification and OMZ intensity in the ETNP and ETSP during the past 1200 years. Quantifying the degree to which OMZ intensity fluctuates and the time scales of these variations is critical in assessing how they may change in response to future changes in climate [*Deutsch et al*., 2014].

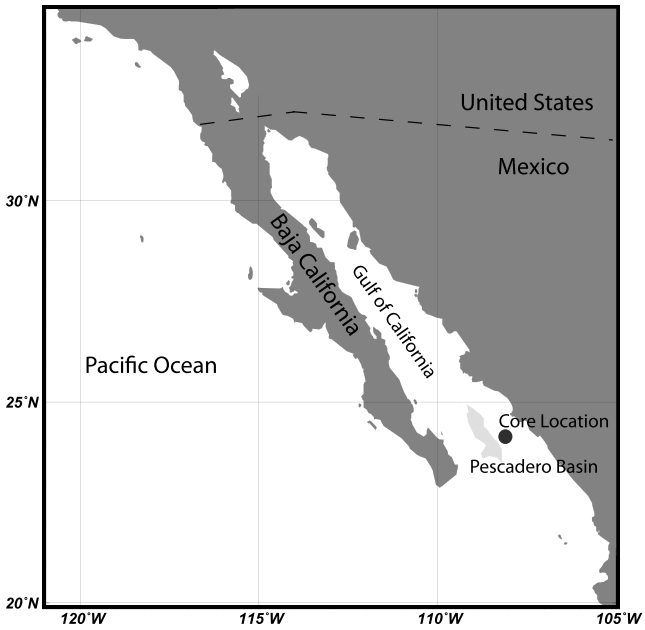

Figure 1. A map of the study region. Pescadero Basin, near the mouth of the Gulf of California and the Pacific Ocean, is shaded gray. The coring location along the Pescadero Slope is represented by the black dot.

A common paradigm is that as the climate warms, O_2 becomes less soluble in seawater and the upper ocean becomes more stratified, reducing ventilation, with both of these processes resulting in a decline in dissolved O_2 in the ocean interior [*Keeling et al*., 2010]. In the eastern tropical Pacific, a 10–20% decline in dissolved O_2 has been observed over the last several decades [*Stramma et al*., 2008; *Bograd et al*., 2008; *McClatchie et al*., 2010] and a 50 year time series of dissolved O_2 also reveals a recent expansion of OMZs globally beginning in ~1990 [*Stramma et al*., 2008]. This has prompted investigations examining fluctuations in the intensity of the ETNP OMZ using paleoceanographic proxies to evaluate decadal and centennial trends over longer time periods [*Deutsch et al*., 2014; *Tems et al*., 2015]. Recent studies indicate that over the last 150 years the ETNP OMZ has been contracting, with the exception of the last 20 years where intensification has occurred. *Deutsch et al*. [2014] attribute this contraction to a reduction in the intensity of the trade winds in a warming climate, which results in a deepening of the low-latitude thermocline. The study presented here builds on the work of *Deutsch et al*. [2014] and *Tems et al*. [2015] using high-resolution laminated sediment records to evaluate if the recent trends and range of OMZ intensity variations are representative of the ETNP on centennial and millennial scales and what additional factors may influence fluctuations in the OMZ on these longer time scales.

Laminated sediments provide excellent high-resolution records of paleoceanographic and paleoclimatic conditions. The $\delta^{15}N$ of bulk sedimentary organic matter (where $\delta^{15}N_{sed}‰ = [(^{15}N/^{14}Nsample)/(^{15}N/^{14}Nstandard) - 1] \times 1000$ and the standard is atmospheric N_2) is used as a proxy for changes in water column denitrification. Water column denitrification is tightly coupled to OMZ oxygen concentration in this region of the ETNP [*Sigman et al*., 2005], and thus, $\delta^{15}N_{sed}$ is a useful tracer of OMZ conditions. Assumptions inherent in the use of sedimentary N isotopes as a proxy for OMZ intensity include the following: if complete nitrate utilization occurs in the photic zone [*Altabet and Francois*, 1994] and if $\delta^{15}N_{sed}$ is not diagenetically altered in the water column and sediments [*Altabet et al*., 1999; *Lehmann et al*., 2002; *Thunell et al*., 2004; *Prokopenko et al*., 2006; *Deutsch et al*., 2014; *Tems et al*., 2015]. In environments with high sedimentation rates and low oxygen concentrations the isotopic value of water column nitrate matches the values recorded in core-top sediments [*Thunell et al*., 2004]. Additionally, studies indicate that under low oxygen conditions, nitrogen isotopes are not preferentially fractionated despite significant degradation of organic matter [*Prokopenko et al*., 2006]. As discussed in *Deutsch et al*. [2014] and *Tems et al*. [2015], we believe that all these criteria are met at the Pescadero Slope site.

Organic carbon export and subsequent consumption of oxygen through remineralization has been shown to be an important factor controlling denitrification rates [*Ward et al*., 2008, 2009; *Babbin et al*., 2014]. We indirectly assess the relationship between carbon export and OMZ intensity at the Pescadero Slope (Figure 1) by examining the temporal patterns of bromine:chlorine elemental ratios (Br/Cl) and comparing this record with the content of organic carbon downcore. Nondestructive X-ray fluorescence (XRF) analysis provides records of elemental concentrations at unprecedented resolution. Bromine concentration in sediments is thought to be fundamentally controlled by marine organic carbon [*Hendy et al*., 2015; *Ziegler et al*., 2008; *Price and Calvert*, 1977] and seawater concentrations. The seawater component can be accounted for by normalizing Br counts to chlorine [*Ziegler et al*., 2008]. This study also provides measurements of weight

percent organic carbon (wt % C_{org}) in the sediments to ensure the validity the Br/Cl proxy. Due to the prevalence of diatoms and other siliceous phytoplankton in the tropical Pacific upwelling zones, we also investigate the relationship between $\delta^{15}N_{sed}$ and wt % biogenic silica (bSi). In these regions, biogenic silica accumulation can be used to establish a lower limit of primary productivity and carbon export [*Pichevin et al*., 2012]. In this study we directly compare temporal trends and periodicities within Br/Cl, wt % C_{org}, wt % bSi, and $\delta^{15}N_{sed}$ to investigate the time-frequency relationship between these proxies of export production and OMZ intensity.

2. Study Site

This study focuses on cores collected from the eastern slope of the Pescadero Basin in the mouth of the Gulf of California (Figure 1). The Gulf of California is an elongate basin, surrounded by land to the north, west, and east, and opens to the Pacific Ocean in the south. In the fall, the Pacific High-Pressure System and the Intertropical Convergence Zone (ITCZ) migrate south toward the equator and the winds intensify. As this occurs, the strength and prominent direction of the winds change from weak southeastern winds to strong northwestern winds [*Douglas et al*., 2007]. The strong northwestern winds cause Ekman transport in the Gulf, resulting in intensified upwelling and stimulating high productivity on the eastern side of the Gulf from November to March [*Staines-Urías et al*., 2009; *Douglas et al*., 2007]. Biogenic silica fluxes in the Gulf are highest during this time of year [*Thunell et al*., 1994]. High productivity coupled with moderate rates of deep thermohaline ventilation results in the formation of a well-developed oxygen minimum zone between 100 and 800 m [*Fernández-Barajas et al*., 1994]. The OMZ impinges on the basin slope where organic-rich (2–5 wt % C_{org}) laminated sediments with elevated $^{15}N/^{14}N$ are found. C:N ratios of 9–11, a zero intercept plot of weight percent nitrogen versus weight percent carbon [*Tems et al*., 2015], and particulate organic matter $\delta^{13}C$ values of −22.1 to −21.2‰ all indicate that the signal is predominantly marine organic matter. Previous studies have used nitrogen isotopes from sediment cores in the central and northern Gulf of California to investigate climatic variability during deglaciation and the early Holocene [*Pride et al*., 1999].

The seasonal and long-term dynamics of water mass mixing in the Gulf of California are dominated by dynamics within the eastern Pacific Ocean [*Lavín and Marinone*, 2003], making it an ideal location to study variations in the ETNP OMZ. Tropical surface water (TSW) and subtropical subsurface water (SSW) is advected from the ETNP into the Gulf during the summer [*Pride et al*., 1999; *Staines-Urías et al*., 2009; *Collins et al*., 1997] below 200 m [*Lavín and Marinone*, 2003; *Pride et al*., 2009]. Gulf of California Water forms in the northern Gulf and outflows in the upper 250 m along the western margin [*Staines-Urías et al*., 2009; *Lavín and Marinone*, 2003].

3. Sampling and Analytical Methods

3.1. Core Collection

One multicore (PESC-MC1, 64.5 cm) and two gravity cores (PESC-GC1, 138 cm, and PESC-GC3, 204 cm) were collected in 2009 from the slope of Pescadero Basin. PESC-MC1 was collected at 24°16.88′N and 108°11.79′W in 616 m water depth. PESC-GC1 and PESC-GC3 were collected at 24°16.160′N, 108°11.599′W and 24°16.759′N, 108°11.700′W and at 601 m and 620 m, respectively. At the time of coring, bottom water [O_2] was $<0.5\ \mu M$ at these locations [*Tems et al*., 2015]. Water column and sediment pore water chemistry at this site are described in *Chong et al*. [2012], *Prokopenko et al*. [2011], and *Townsend-Small et al*. [2014].

3.2. Age Model

The multicore, PESC-MC1, preserved the sediment-water interface and the deposition of the most recent sediments. To align the $\delta^{15}N_{sed}$ records from PESC-MC1 and PESC-GC3, weight percent total carbon, $\delta^{13}C_{sed}$ total carbon, and paleomagnetic data were used to correlate PESC-MC1 to PESC-GC1 and PESC-GC1 to PESC-GC3 (supporting information Figure S1). The age model for the cores was constructed by combining and cross-correlating ^{210}Pb measurements (obtained by gamma spectroscopy), accelerator mass spectrometry AMS ^{14}C measurements, and varve counts. The ^{210}Pb age model, developed by plotting integrated mass and ^{210}Pb and fitting an exponential decay regression to the data (supporting information Figure S2) [*Deutsch et al*., 2014; *Tems et al*., 2015], resulted in a sediment accumulation rate of 77.4 mg cm^{-2} yr^{-1}, which was applied to the first 135 years of PESC-MC1. The age model for the remainder of PESC-MC1 and all of PESC-GC3 is based on a linear regression of calibrated ^{14}C calibrated ages.

Table 1. Original ^{14}C Ages (BP) Measured at UC Irvine, Original Sample Depth, and the Corrected Ages (A.D.) After Applying a Local Reservoir Effect ($\Delta R = 508 \pm 30$) for PESC-MC1 and PESC-GC3

	^{14}C Age Model Data	
Average Depth (cm)	Uncorrected ^{14}C Age (B.P.)	ΔR Corrected Year (A.D.)
	PESC-MC1	
5.25	540 ± 20	not applicable
18.45	985 ± 20	1860 ± 43.5
41.85	1015 ± 20	1818 ± 40
51.75	1015 ± 20	1818 ± 40
	PESC-GC3	
41.85	1090 ± 20	1733 ± 43
46.5	1140 ± 20	1670 ± 37.5
48.45	1180 ± 20	1628 ± 44.5
58.95	1240 ± 20	1576 ± 48
72.45	1235 ± 20	1580 ± 48
79.9	1440 ± 20	1416 ± 32
85.75	1320 ± 20	1497 ± 31.5
96.55	1410 ± 20	1437 ± 25.5
102.85	1440 ± 20	1416 ± 32
104.5	1420 ± 20	1431 ± 27
112.15	1590 ± 20	1303 ± 30
121.35	1530 ± 20	1352 ± 36.5
133.05	1540 ± 20	1345 ± 25.5
142.05	1700 ± 20	1219 ± 40.5
146.8	1725 ± 20	1194 ± 46.5
157.65	1800 ± 20	1113 ± 47.5
167.5	1795 ± 20	1117 ± 48
178.65	1910 ± 20	1001 ± 39.5
188.55	1985 ± 20	927 ± 50.5
193.05	1950 ± 20	962 ± 45
197.65	2035 ± 20	865 ± 54
202.45	2075 ± 20	821 ± 51.5

The ^{14}C age model is based on the analysis of 26 samples of sedimentary organic matter. The samples were pretreated with an acid-base-acid washing procedure [*Olsson*, 1986], graphitized [*Xu et al.*, 2007], and analyzed for organic matter AMS dating [*Southon and Santos*, 2004, 2007] at the Keck Carbon Cycle AMS Facility at the University of California (UC) Irvine. Additional samples were also measured without undergoing acid/base pretreatment procedures, and dates of treated and nontreated samples of the same interval were found to be within analytical error of each other. The ^{14}C measurements were corrected for preparation backgrounds and isotopic fractionation according to conventions of *Stuiver and Polach* [1977], and a marine correction using Calib 7.1 [*Stuiver and Reimer*, 1993], including a correction for local reservoir age (relative to the global ocean reservoir age, ΔR) of 508 ± 30 years, was applied (Table 1). This correction was estimated by averaging the radiocarbon ages obtained from PESC-MC1 older than 1950 AD ($n = 3$) after each was corrected by the global reservoir age for the year the sediment was deposited as determined by the ^{210}Pb age model. The global reservoir age was determined from Marine13 [*Reimer et al.*, 2013], and error in ΔR was calculated as the standard deviation between the average reservoir corrections from PESC-MC1. Independent analysis of radiocarbon ages obtained from PESC-GC3 suggested a reservoir age within error of that calculated for PESC-MC1. The calibrated ages were compared to the integrated mass (related to depth in the core by porosity, which corrects for the effect of compaction) and fit with a linear model ($r^2 = 0.98$, $P < 0.001$), which yielded an average sediment accumulation rate of 77.4 mg cm^{-2} yr^{-1} (Figure 2a). This $\Delta^{14}C$-derived value is identical to the sedimentation rate derived from the ^{210}Pb model of PESC-MC1. The reservoir age correction determined from the post-1950 sediments was assumed to be constant and apply through the depth of the gravity core.

The validity of the radiocarbon age model is further supported by laminae counts. We counted 796 laminae couplets, defined as one light and one dark band as viewed on high-resolution images and X-radiographs, in what is determined by our radiometric isotope age model to be 721 years (Figure 2b), which illustrates that within 10%, laminae couplets are annual varves. Multiple counts were completed of the same core section to demonstrate that counting was reproducible within 1.5% (12 years).

3.3. Sediment Chemistry Analytical Techniques

PESC-MC1, PESC-GC1, and PESC-GC3 were split lengthwise and sampled at 3 mm resolution. PESC-MC1 and PESC-GC1 were digitally scanned at high resolution, and PESC-GC3 was x-radiographed and imaged (supporting information Figure S3) confirming the presence of laminated sediments throughout all three cores. Measurements of $\delta^{15}N$, percent total organic carbon (%TOC), and weight percent biogenic silica were made on sediment splits from PESC-MC1 and PESC-GC3. Measurements of total carbon $\delta^{13}C$ and wt % total carbon were made on sediment splits from PESC-MC1, PESC-GC1, and PESC-GC3 to correlate the three cores.

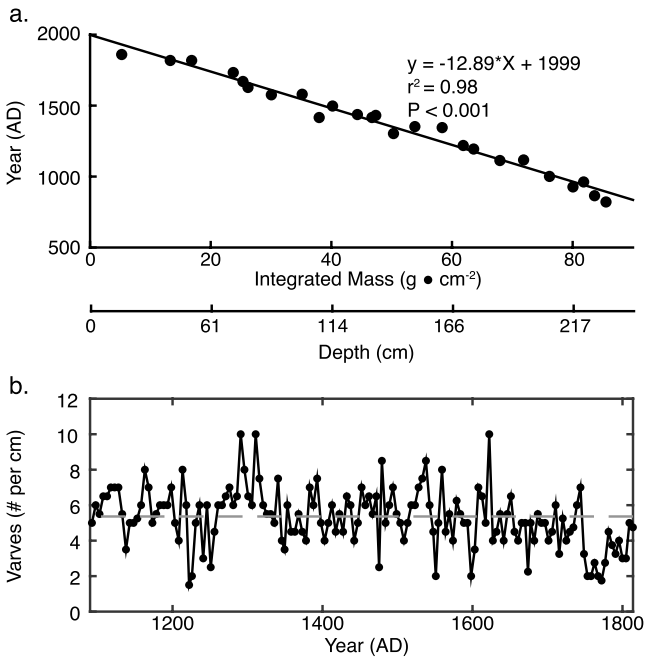

Figure 2. The age model constructed for PESC-GC3. (a) Radiocarbon measurements were calibrated using Calib 7.1 with a reservoir age (ΔR) of 508 ± 30 years. This age is compared to the integrated mass, which relates to depth in the core by taking porosity of the sediments into consideration therefore correcting for compaction. The sedimentation rate is 77.4 mg cm^{-2} yr^{-1}. Approximate depth is included as a secondary *x* axis for comparison to integrated mass values. (b) Dark-light couplet counts were completed by dividing the core into 1 cm bins. The number of couplets per 1 cm bin is compared to age as calculated from the radiocarbon age model. If sedimentation rate is linear, as assumed by the age model, 5.2 couplets should be present in each centimeter (dashed horizontal line) if these couplets represent varves.

Individual samples were prepared for bulk $\delta^{15}N_{sed}$ by drying and grinding to a fine powder. The samples from PESC-MC1 were analyzed with a PDZ Europa ANCA-GSL elemental analyzer interfaced to a PDZ Europa 20-20 continuous flow isotope ratio mass spectrometer (IRMS) at the UC Davis Stable Isotope Facility. The references used to normalize the data were G-11 (nylon, $\delta^{15}N$ of −9.77‰), G-12 (glutamic acid enriched, $\delta^{15}N$ of 45.31‰), G-13 (bovine liver, $\delta^{15}N$ of 7.72‰), and G-9 (glutamic acid, $\delta^{15}N$ of −4.26‰). PESC-GC3 samples were measured for $\delta^{15}N_{sed}$ at the University of South Carolina on a Euro Elemental Analyzer interfaced to a GV Isoprime continuous flow IRMS. The reference standards used to normalize the data were N-1 ($\delta^{15}N = 0.4$‰), N-2 ($\delta^{15}N = 20.41$‰), N-3 ($\delta^{15}N = 4.7$‰), and USGS-40 ($\delta^{15}N = -4.52$‰). An interlaboratory calibration showed that the measurements at each facility were within analytical error of each other. Uncertainty was determined by averaging the standard deviation between replicate samples ($n = 15$) and was calculated to be 0.17‰.

Biogenic silica (bSi) analyses were run at the University of Southern California (USC) using a hot sodium bicarbonate leaching method [*DeMaster*, 1979, 1991; *Strickland*, 1968]. For each sample, 10 to 12 mg of powdered sediment were measured into 50 mL plastic centrifuge tube and 50 mL of 5% (weight/volume) sodium bicarbonate was added. The centrifuge tube was then placed in an 80°C bath for 5 h. Each sample was mixed every 30 min, and 0.5 mL aliquot subsamples were taken at 3, 4, and 5 h intervals. Each subsample was neutralized with 0.235 *M* hydrochloric acid and analyzed colorimetrically on a spectrophotometer. Measured samples were corrected to account for dilution factors and changes in volume in the centrifuge tube due to sampling. The corrected concentration was computed for each subsample time point and fitted with a linear regression. The *y* intercept was used to calculate the biogenic silica concentration and subsequently the weight percent biogenic silica. Error was calculated by averaging the standard deviation between replicate samples and was found to be ±0.15%.

Five to 8 mg of powdered sediment were packaged into tin capsules and analyzed for total carbon $\delta^{13}C$ and weight percent total carbon at USC on a Costech ECS 4010 elemental analyzer interfaced to a Picarro G2131-i cavity ring down spectrometer. For this analysis the standard used was L-glutamic acid (USGS 40) with $\delta^{13}C_{VPDB} = -26.39 \pm 0.04$‰ and a carbon mass fraction of 40.8%. Weight percent inorganic carbon was also measured and used to calculate weight percent organic carbon. The inorganic carbon measurements were made on the Picarro G2131-i cavity ring down spectrometer using an Automate device to acidify the sample. For this analysis, 14 to 335 mg of powdered sample were placed in a glass test tube, which was evacuated using a vacuum pump, and preacidified with 1 mL of 10% phosphoric acid (from which CO_2 had been removed by bubbling the solution with N_2 gas for 20 min). When analyzed, the Automate injects an additional 3 mL of 10% phosphoric acid and the CO_2 that is released from the sample is collected and analyzed using the Picarro. The standards used for the inorganic carbon analyses were OPT Calcite ($\delta^{13}C_{VPDB} = 2.47$

± 0.01 and 12.002% C) and AR15 ($\delta^{13}C_{VPDB} = -9.65 \pm 0.03$). Weight percent organic carbon was calculated as the difference between wt % total and wt % inorganic C.

Due to very small amounts of inorganic carbon in many samples, an alternative acid fumigation method was also used to remove carbonate for measurement of wt % C_{org}. This method involved weighing 7–10 mg of ground sediment into silver capsules, acidifying the samples by adding 0.15 mL of deionized water to each sample and placing the samples in a desiccator containing a beaker with 50 mL of reagent grade HCl for 8 h, after which the samples where placed in an oven to dry, packaged in an additional tin cup, and measured on a Costech ECS 4010 elemental analyzer interfaced to a Picarro G2131-i. For this analysis the standard used was L-glutamic acid (USGS 40, 40.8% mass fraction C). The two methods for measuring wt % C_{org} and $\delta^{13}C_{org}$ are within error of each other.

X-ray florescence (XRF) of contiguous sections of PESC-GC3 was conducted using an AvaaTech XRF Core-Scanner at ETH Zurich. The core-scanner X-ray source was a Rhodium anode and was calibrated using an internal standard, SARM4. Chlorine and bromine elemental scans were completed at 10 kV and 30 kV, respectively. These elemental counts measured were well above background to ensure the validity of the measurements and potential. Counts were conducted over 20 s time intervals at 0.5 mm intervals.

We also assessed the concentration of magnetic particles, their grain size distribution, and variations in the percentage of various magnetic minerals in order to accurately match PESC-MC1 and PESC-GC1. Such measurements have been used routinely [*Bloemendal et al.*, 1988; *King and Channell*, 1991] as proxies for variations in bulk clastic sedimentology (clastic concentration, grain size, and mineralogy). For this analysis, PESC-MC1 and PESC-GC1 were sampled discretely and contiguously using 2 cm^3 samples. The bulk magnetic susceptibility (chi) of each sample was measured at USC. Two artificial remanences were then applied in sequence, an anhysteretic remanence (ARM, applied in 0.05 mT applied field and 100 mT af field), and a saturation isothermal remanence (SIRM, applied at 1000 mT steady field). Both remanences were af demagnetized sequentially in fields of 10 mT, 20 mT, and 40 mT. Variations in chi, ARM, and SIRM intensity were used to assess the concentration of magnetic particles in the sediments (and by proxy, clastic sediment concentration). The ratios ARM/chi, ARM20/0, and SIRM20/0 were used to estimate the percentage of finer-grained magnetic particles (and by proxy, clastic grain size variability). All six parameters were plotted for cores PESC-MC1 and PESC-GC1 and compared. Five clear parameter highs/lows could be correlated between the cores, and there was a simple linear relationship identified between them. The correlations indicate that PESC-MC1 had 30 ± 2 cm of sediment not present in PESC-GC1. Presumably, that sediment was lost from PESC-GC1 during coring.

3.4. Spectral Analysis

To identify periodicities in the Pescadero sediment chemistry data, we performed spectral analysis using a Lomb-Scargle Fourier transform [*Lomb*, 1976; *Scargle*, 1982, 1989] in combination with a Welch-Overlapped-Segment-Averaging procedure [*Welch*, 1967; *Schulz and Stattegger*, 1997; *Schulz and Mudelsee*, 2002; *Khider et al.*, 2014]. We chose this method since our record is not uniformly spaced in time and other methods would require the data to be interpolated, resulting in dependent data points and potentially biased results [*Schulz and Stattegger*, 1997; *Khider et al.*, 2014]. The Lomb-Scargle periodogram weights the data on a "per point" basis instead of a "per time interval," eliminating the need for interpolation. A mathematical formulation of the methods is summarized in *Khider et al.* [2014].

4. Results

Our $\delta^{15}N_{sed}$ record from the Pescadero Slope shows fluctuations between 8.1 and 10.4‰ over the past 1121 years, with an overall mean value of 9.28 ± 0.34‰ ($n = 739$, Figure 3). We find no consistent long-term trend through the record. Variations between low $\delta^{15}N_{sed}$ values (interpreted as a less intense OMZ) and high $\delta^{15}N_{sed}$ (a more intense OMZ) occur rapidly and are generally followed by more gradual declines in OMZ intensity (from high $\delta^{15}N_{sed}$ to low $\delta^{15}N_{sed}$) (Table 2). We assessed this quantitatively by dividing the $\delta^{15}N_{sed}$ record into 10 distinct cycles and calculating the rate of increase in $\delta^{15}N_{sed}$ to maximum values and the rate of decrease to minimum values. Each cycle was defined as encompassing the full transition between an intensification/relaxation of the OMZ that lasted longer than 40 years after a 20 year weighted average was applied to the record. A 20 year weighted average was applied to smooth the $\delta^{15}N_{sed}$ record

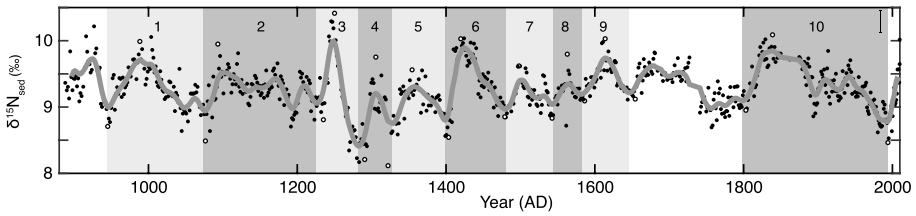

Figure 3. $\delta^{15}N_{sed}$ (‰) from the Pescadero Slope multicore and gravity core compared to year (A.D.) as calculated by ^{210}Pb and ^{14}C age models. Individual data points are represented by black dots, while a 20 year smoothed curve is shown in gray. The record has been divided into 10 sections, in which each includes intensification (increase in $\delta^{15}N_{sed}$) and deintensification (decrease in $\delta^{15}N_{sed}$) that occurred over a minimum of 35 years. Original data points used to define maxima and minima are indicated on the figure as white dots (outlined in black). The section between 9 and 10 was not included in this analysis since there are missing data in this section.

and define minima and maxima objectively. In nine of 10 intervals, OMZ expansion or intensification ($\delta^{15}N_{sed}$ increase) occurred more quickly than OMZ contraction. The one interval in which this pattern was not observed (cycle 3) is an atypical fluctuation in the record and represents the largest variation in the intensity of the OMZ. In cycle 3, the rate of OMZ expansion is quite similar to the OMZ contraction rate. Considering all 10 cycles, the average rate of $\delta^{15}N_{sed}$ increase was 0.025 ± 0.011‰ yr^{-1} and the average rate of $\delta^{15}N_{sed}$ decrease was 0.015 ± 0.012‰ yr^{-1} (where ± is standard deviation of the mean). Thus, the increase in isotopic values occurs 1.7 times faster than the rate of isotope decline. Gradients calculated using minima and maxima in the data (rather than the smoothed curve) show similarly rapid rates of $\delta^{15}N_{sed}$ increase and slower rates of $\delta^{15}N_{sed}$ decrease (Table 2). In this case, the rate of increase is similarly 2 times greater than the rate of decrease.

Table 2. Assessment of OMZ Fluctuations Based on Changes in $\delta^{15}N_{sed}$[a]

Section[b]	Slope (L-H)[b] (‰ yr^{-1})	Slope (H-L)[b] (‰ yr^{-1})
	20 Year Weighted Average	
1	0.0169	0.0086
2	0.0237	0.0037
3	0.0415	0.0458
4	0.0353	0.0203
5	0.0189	0.0121
6	0.0432	0.0169
7	0.0186	0.0091
8	0.0141	0.0091
9	0.0171	0.0157
10	0.0187	0.0069
Average	0.0248	0.0148
	Original Data	
1	0.0297	0.0170
2	0.0875	0.0080
3	0.1068	0.0545
4	0.1032	0.0996
5	0.0447	0.0207
6	0.0911	0.0196
7	0.0236	0.0133
8	0.0472	0.0302
9	0.0340	0.0225
10	0.0318	0.0105
Average	0.0600	0.0296

[a]Each data section is indicated (refer to Figure 3 for exact location) and the slope (absolute value) calculated between $\delta^{15}N_{sed}$ local minima and maxima (slope L-H) and $\delta^{15}N_{sed}$ local maxima and minima (slope H-L). This is calculated for each section after a 20 year smoothed curve was applied and for the original data presented in Figure 3. These calculations indicate that there is an average increase of 0.025 ± 0.11‰ yr and an average decrease of 0.015 ± 0.12‰ yr when the 20 year low-pass filter is applied and an average of increase of 0.060 ± 0.033‰ yr and decrease of 0.030 ± 0.28‰ yr based on the original data set.

[b]Absolute value of the slope between L (low $\delta^{15}N_{sed}$ values) and H (high $\delta^{15}N_{sed}$ values) and vice versa.

Weight percent (wt %) organic carbon in the sediments varies between 2.8 and 4.3% with an average of 3.5% and uncertainty of ±0.05% ($n = 193$, Figure 4b). As with the $\delta^{15}N_{sed}$ values, there is no overall temporal trend in wt % C_{org}. High-resolution measurements of C_{org} content between 1518 and 1640 A.D. indicate that Br/Cl counts track C_{org} trends (Figure 4b) and supporting information Figure S4), suggesting that Br/Cl can be used as a proxy for the preservation of C_{org} at the Pescadero Slope site. General coherence is also observed between $\delta^{15}N_{sed}$ and wt % C_{org} on both interannual and decadal time scales in this continuous section of measurements. For most of this section, changes in the magnitude of $\delta^{15}N_{sed}$ are met with near-synchronous changes in wt % C_{org} of the same scale although there are periods (1540–1570, for example) where

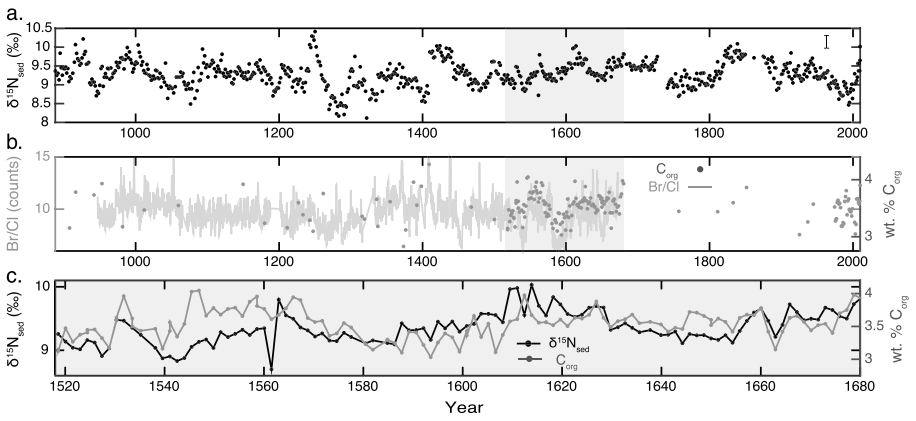

Figure 4. Geochemical measurements from sediment splits from cores PESC-MC1 and PESC-GC3 compared to the year (A.D.) the sediments were deposited. (a) $\delta^{15}N_{sed}$ (‰). Uncertainty was calculated to be 0.17‰ for each measurement and is represented by an error bar in the top right corner. (b) Weight percent organic carbon (right *y* axis, dark gray). Uncertainty is ±0.05% and is encompassed within the size of the data point. Br/Cl data are shown in light gray (left *y* axis). The ratio between Br and Cl has been normalized by their elemental ratios in seawater (0.0034). (c) A comparison between $\delta^{15}N_{sed}$ (‰) and wt % C_{org} from 1518 to 1860 A.D. These data are highlighted in gray in Figure 4a and 4b. When wt % C_{org} is directly compared to $\delta^{15}N_{sed}$ between 1680–1574 A.D. and 1540–1518 A.D., a significant positive relationship exists (wt % $C_{org} = 0.62 \times \delta^{15}N_{sed} + 7.2$; $r^2 = 0.26$, $P = <0.001$). While there is also a significant positive relationship between the two parameters between 1573 and 1541 A.D., less variance is accounted for (wt % $C_{org} = 0.45 \times \delta^{15}N_{sed} + 7.5$; $r^2 = 0.12$, $P = <0.001$).

the proxies exhibit the same trend but an increased difference between measurement values, after which measurements return to showing similar short-term variation (Figure 4c).

Biogenic silica (bSi) content of the sediments varies between 2.6 and 21.8 wt % over the last ~1200 years; however, as seen in the wt % C_{org} record, there is no systematic long-term trend over this time period. The single high wt % bSi value is ~3 times greater than the mean bSi value (7 wt %) as all other measurements were between 3 and 11 ± 0.2%. When directly compared $\delta^{15}N_{sed}$ and wt %, bSi are positively correlated but do not exhibit a significant relationship ($P > 0.05$) (supporting information Figure S5).

Spectral analysis of the Pescadero Slope $\delta^{15}N_{sed}$ and Br/Cl XRF counts reveals decadal, multidecadal, and centennial periodicities. Peaks at or above the 95% confidence level (Figure 5a) are found in the $\delta^{15}N_{sed}$ record at 50, 65, 86, 102, and 230 years. Periodicities in the Br/Cl counts are observed at 18, 28, 48, 65, 129, 181, and 242 years (Figure 5b).

5. Discussion

5.1. Denitrification and Carbon Production and Export

Climate variations influence denitrification and the extent of OMZs on glacial to interglacial time scales [*Altabet et al.*, 1995; *Ganeshram et al.*, 1995, 2000] and have been hypothesized to influence denitrification changes in the Pleistocene [*Liu et al.*, 2008]. High-resolution studies revealing decadal- to centennial-scale fluctuations in the OMZ during the Holocene and the drivers of these fluctuations have not been assessed for the ETNP. The fluctuations in $\delta^{15}N_{sed}$ values from Pescadero Slope during the last millennium range from a maximum of 10.4‰ to a minimum of 8.1‰ and exhibit rapid increases in OMZ intensity followed by gradual declines (Figure 3). We hypothesize that the asymmetry between oxygen depletion and reoxygenation of ETNP OMZ may be due to the coupling of upwelling, organic carbon production, export, and rapid O_2 consumption outpacing subsurface ventilation. This asymmetry was also captured by a general circulation model (GCM) with an explicit nitrogen cycle, which used the first 200 years of the Pescadero Slope record to test hypothesized mechanisms driving OMZ intensity [*Deutsch et al.*, 2014].

Lower resolution, longer-term records from the center of ETNP and Arabian Sea OMZs indicate that while mean $\delta^{15}N_{sed}$ values are lower during glacial periods, a similar maximum to minimum range of values (2–3‰) is observed [*Ganeshram et al.*, 1995]. The ETNP region is characterized by values between 5.5 and

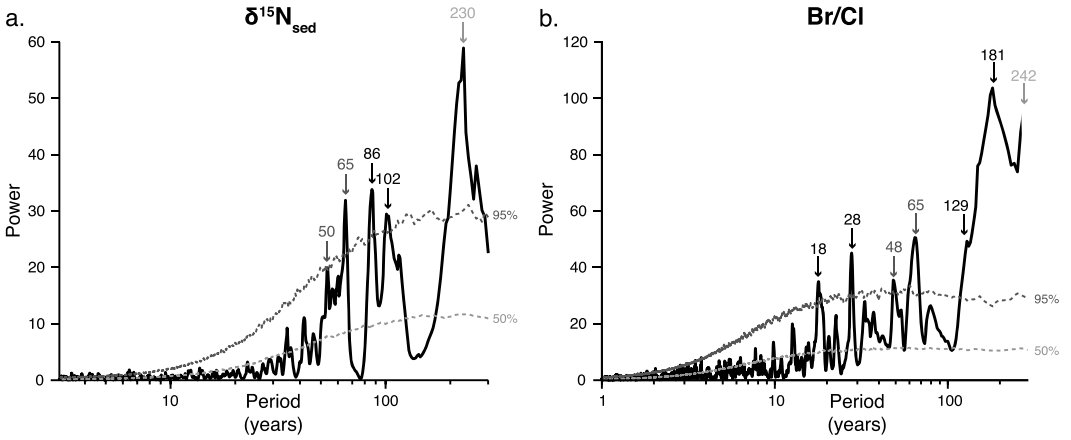

Figure 5. (a) Spectral analysis of $\delta^{15}N_{sed}$ data. Peaks representing 50, 65, 86, 102, and 230 years are observed in the record with greater than 95% confidence. (b) Spectral analysis of Br/Cl data. Similar peaks are seen at 48, 65, and 242 years. Similar peaks are seen at 48, 65, and 242 years. Similarities are highlighted in dark gray (to represent the Pacific Decadal Oscillation) and light gray (to represent Suess (deVries) solar cycle).

8.2‰ during glacial periods [*Ganeshram et al*., 1995]. This suggests that similar mechanisms influencing the degree of variation in denitrification in OMZs are present during both the Holocene and glacial periods, with each climate state defined by different limits of denitrification intensity. $\delta^{15}N_{sed}$ records from the central and northern Gulf of California reveal a greater range of variation in values; however, this has been suggested to be related to increased nitrogen isotopic values in Central Gulf Water and terrestrial input [*Pride et al*., 1999], which are specific influences to the central and northern Gulf.

To investigate what factors could be contributing to the observed late Holocene range of denitrification intensity, we investigate the relationship between denitrification and carbon export/preservation by comparing high-resolution sections of $\delta^{15}N_{sed}$ and wt % C_{org} and periodicities in $\delta^{15}N_{sed}$ and Br/Cl counts. Coherence between $\delta^{15}N_{sed}$ and wt % C_{org} on interannual, decadal, and centennial time scales in a continuous section of high-resolution measurements (Figure 4c) suggests a coupling between denitrification and organic carbon preservation. We hypothesize that C_{org} preservation may reflect C_{org} production/export. In addition to a direct comparison of independent sediment proxies, spectral analysis identified similar periodicities in both the $\delta^{15}N_{sed}$ and Br/Cl (a proxy for C_{org}) records. Analogous periodicities (50, 65, and 230 years in $\delta^{15}N_{sed}$ and 48, 65, and 242 years in Br/Cl) suggest that similar mechanisms are influencing both carbon preservation and denitrification at the Pescadero Slope over the past 1200 years. It seems likely that this tight coupling represents changes in C_{org} export and its impact on both denitrification and C_{org} preservation.

The limited range of fluctuation observed in $\delta^{15}N_{sed}$ may be influenced by feedbacks associated with organic carbon export. Increased production and export of organic carbon from the photic zone could result in increased denitrification. Increased denitrification would in turn reduce the availability of nitrate, which would reduce primary production and export of organic matter from the photic zone due to upwelling of more nutrient-depleted waters. This would reduce carbon export and denitrification resulting in the accumulation of nutrients, which would then stimulate productivity when upwelled into the photic zone. We recognize that deviation in the coherence of the $\delta^{15}N_{sed}$ and wt % C trends also implies that additional feedbacks and natural fluctuations add complexity to ETNP OMZ system, which could include remote ventilation. Coupling between productivity (export) and denitrification has also been identified in the eastern tropical South Pacific [*Agnihotri et al*., 2008]. Testing and quantifying this mechanism in a GCM is a goal for future work.

Since diatoms and silicoflagellates contribute to export and productivity at the Pescadero Slope site, we also investigated the relationship between wt % bSi and $\delta^{15}N_{sed}$. This relationship, however, is not statistically robust at this site (supporting information Figure S5). This weak correlation could be due to the following: (1) the $^{15}NO_3^-$ signal is entirely due to transport from lower latitudes of the ETNP OMZ and hence is decoupled from local production and export, (2) variable amounts of remineralization of bSi in the water column attenuate the signal in sediments, (3) dissolution/diagenesis of bSi in the sediments occurs after

deposition, and/or (4) bSi accumulation represents diatom bloom events that do not represent OMZ conditions. A significant portion of bSi produced in the Gulf is dissolved within the upper water column (above 200 m) [*Thunell et al*., 1994; *Pride et al*., 1999] which might alter the bSi signal in sediments. Weight % bSi may better serve as a proxy for diatom/siliceous plankton bloom events rather than overall net primary productivity. This suggests that wt % C_{org} in the sediments might be the more reliable proxy for assessing past changes in primary productivity on Pescadero Slope.

5.2. The Pacific Decadal Oscillation and Solar Forcing

Spectral analysis provides a method to determine if there are significant periodicities in the data, and this in turn can be used to assess what factors drive OMZ intensity during the late Holocene. Holocene marine and lacustrine sediments, tree ring, fish populations, and North American surface temperature studies have shown periodicities between 50 and 70 years [*Baumgartner et al*., 1992; *Meko*, 1992; *Sharp*, 1992; *Schlesinger and Ramankutty*, 1994; *Thurow and Schaaf*, 1995; *Minobe*, 1997; *Pike and Kemp*, 1997; *MacDonald and Case*, 2005], similar to the highly significant ~50 and ~65 year frequencies identified in the $\delta^{15}N_{sed}$ record and the ~48 and ~65 years periodicities in the Br/Cl records (Figures 4a and 4b). This frequency of variability is thought to relate to Pacific basin-wide changes in atmospheric and oceanic circulation, known as the Pacific Decadal Oscillation (PDO) [*Minobe*, 1997; *Pike and Kemp*, 1997; *Mantua and Hare*, 2002]. PDO has been identified as a dominant periodicity seen in many other Gulf of California proxy records including planktonic foraminifera $\delta^{18}O$ records from the Pescadero Basin [*Staines-Urías et al*., 2009], diatom mats [*Pike and Kemp*, 1997], and $\delta^{15}N$ from Alfonso Basin [*Ricaurte-Villota et al*., 2013]. *Tems et al*. [2015] also found that the PDO drives variations in the transport of elevated $\delta^{15}NO_3^-$ from the ETNP OMZ northward to the California Borderland.

The longer $\delta^{15}N_{sed}$ periodicities of 86, 102, and 230 years could be related to solar activity, more specifically, the Gleissberg and Suess (deVries) cycles. The Gleissberg cycle, traditionally thought to occur at an 80–90 year periodicity and a function of the 11 year Schwabe sunspot cycle, is more complex having a wider frequency band with a double structure of 50–80 and 90–140 year periodicities, than the Suess cycle, which shows variation with a period of 170–260 years [*Ogurtsov et al*., 2002]. While variations in solar irradiance during a sunspot cycle are less than 0.1% [*Burroughs*, 1992], amplification of this signal has been proposed by magnetic processes [*Burroughs*, 1992] or absorption of UV radiation in the atmosphere [*Pike and Kemp*, 1997]. Furthermore, studies involving lake sediment varve thickness (a proxy for wind strength) and $\Delta\delta^{14}C$ (a proxy for solar activity) tree ring records [*Anderson*, 1992] show coherence between changes in the Earth's magnetic field, dominant sunspot cycles, coronal explosions, and PDO periodicities and suggest that it is plausible that solar cycles are influencing climate and ocean circulation patterns in the Pacific [*Pike and Kemp*, 1997].

Other studies have also found that solar forcing is likely influencing the dynamics of the southern Gulf of California. Solar forcing is the inferred mechanism for ~100 and 200 year variations in diatom and silicoflagellate presence/assemblages [*Barron et al*., 2003; *Barron and Bukry*, 2007], and biogenic silica and carbonate accumulation [*González-Yajimovich et al*., 2005], which serve as proxies for productivity. It is proposed that reduced solar irradiance causes cooling of the winter atmospheric temperatures above the southwest U.S., strengthening the atmospheric low and causing an intensification of northwest winds in Gulf and increased biological productivity [*Barron et al*., 2003; *Barron and Bukry*, 2007]. Productivity changes have additionally been linked to latitudinal shifts in the Intertropical Convergence Zone (ITCZ) in the southeastern Gulf (Alfonso Basin), with a progressive equatorward shift of the ITZC over the past 3000 years [*Pérez-Cruz et al*., 2013]. Latitudinal shifts in the ITCZ occurring at centennial periodicities have been recorded in proxies in the Gulf of Mexico [*Poore et al*., 2004] and are associated with changes in solar irradiance, which influence Northern Hemisphere temperatures. We hypothesize that the centennial variability in OMZ intensity at the Pescadero Slope may be related to changes in solar irradiance, which influences North Hemisphere temperatures and atmospheric circulation and results in latitudinal shifts in the ITCZ which in turn impact denitrification and productivity in the region. Shifts in ITCZ latitudinal position have also been suggested as a mechanism influencing centennial-scale variability in the ETSP [*Agnihotri et al*., 2008; *Gutiérrez et al*., 1997].

5.3. Change in O_2 Content

Fluctuations in denitrification intensity are explicitly connected to oxygen concentrations, and therefore, we interpret $\delta^{15}N_{sed}$ values as reflecting changes in the oxygen content of the OMZ. In order to predict how

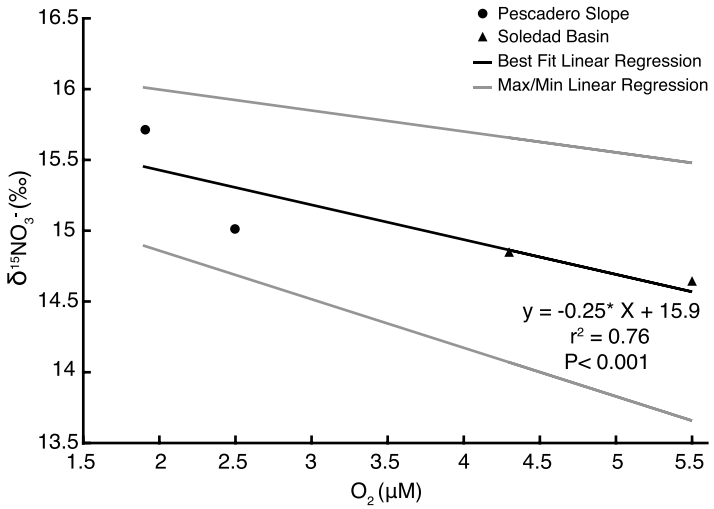

Figure 6. A comparison between the dissolved $\delta^{15}NO_3^-$ (‰) and O_2 content (μM) in the water column at Pescadero (circles) and Soledad Basin (triangles) from the water column [*Townsend-Small et al*., 2014].

oxygen within the ETNP changes relative to fluctuations in $\delta^{15}N_{sed}$ in the ETNP, we compared water column $\delta^{15}NO_3^-$ and O_2 measurements obtained by *Townsend-Small et al*. [2014] from the Pescadero Slope and nearby Soledad Basin (Figure 6). We also avoided using data where O_2 measurements were $<1.5\ \mu M$ due to uncertainty in oxygen measurements at this low level [*Riser and Johnson*, 2008; *Bograd et al*., 2008; *Prokopenko et al*., 2011; *Pierce et al*., 2012; *Townsend-Small et al*., 2014] and where O_2 measurements were $>5.5\ \mu M$ to ensure that denitrification was the dominant processes influencing the fractionation of nitrate isotopes. The significant relationship between $\delta^{15}NO_3^-$ and O_2 ($\delta^{15}NO_3^- = -0.25 \times [O_2] + 15.9$; $r^2 = 0.76$, $P < 0.001$) (albeit derived from only four points) applied to our $\delta^{15}N_{sed}$ values indicates that a 1‰ change in $\delta^{15}NO_3^-$ is equivalent to a $4 \pm 1\ \mu M$ change in $[O_2]$. This interpretation is a simplification of the exact nature of the oxygen-nitrate relationship, and we do not exclude the possibility that other factors may affect the isotope value of nitrate that exits the photic zone as particulate N. These other factors include upwelling from different depths, partial utilization of nitrate, ecosystem structure, and extent and intensity of N fixation. To reduce uncertainty in this relationship, we restricted the water depths analyzed to 150 to 250 m. Water from this depth range has measureable nitrate and is likely from a source of upwelled water to the surface ocean in this region [*Feely et al*., 2008]. Additionally, minimal N_2 fixation has been found in close proximity to the Pescadero site [*White et al*., 2013].

To further assess if a $4 \pm 1\ \mu M$ change in $[O_2]$ per 1‰ change in $\delta^{15}NO_3^-$ is reasonable, we compare the $[O_2]$ rate of decline of $0.13 \pm 0.32\ \mu mol\ kg^{-1}\ yr^{-1}$ in the eastern tropical Pacific [*Stramma et al*., 2008] to the increase in $\delta^{15}N_{sed}$ values for the past 16 years (1.56‰) from our study. Using this method, a 1‰ change of $^{15}NO_3^-$ is equivalent to a change of 1.3 to 4.7 μM O_2, which encompasses the value calculated by directly comparing $\delta^{15}NO_3^-$ and O_2 at the Pescadero Slope and Soledad Basin. In keeping with a simple interpretation of the N cycle in this coastal system, our data implies that over the past 1200 years there have been $>8\ \mu M$ changes in oxygen content in the upper portion of the ETNP OMZ. Some of these changes in oxygen content occurred in as short as 25 years.

Based on our interpretation of changes in $\delta^{15}N_{sed}$, the average O_2 decline in the ETNP is $0.24\ \mu M\ yr^{-1}$ during periods when the ETNP OMZ was expanding. While the current expansion of the ETNP OMZ is not unprecedented at the Pescadero Slope during the last 1200 years, recent observations in the Southern California Borderland indicate that O_2 is declining 7 times quicker ($1.7\ \mu M\ yr^{-1}$) [*Bograd et al*., 2008] than within the ETNP OMZ. This suggests that O_2 declines along western North America, north of the ETNP, may currently be decoupled from OMZ fluctuations and could be the product of changes in ocean chemistry in the North Pacific instead of the ETNP. Changes in ocean chemistry have also been suggested to explain alteration of mixing relationships in the Southern California Borderland [*Tems et al*., 2015] and have significant implications for the region.

6. Conclusions

Eastern tropical North Pacific (ETNP) oxygen minimum zone (OMZ) fluctuations during the last 1200 years are characterized by periods of rapid intensification that are immediately followed by a period of gradual reoxygenation. Intensification is twice as fast as reoxygenation, which is hypothesized to relate to O_2 respiration outpacing physical transport. Coherence between high-resolution measurements of $\delta^{15}N_{sed}$ and weight percent C_{org} and periodicities observed in $\delta^{15}N_{sed}$ and Br/Cl records suggest that similar mechanisms are influencing both carbon production/export and denitrification at the site. Observed periodicities indicate that decadal and centennial variability at the Pescadero Slope could be the result of the Pacific Decadal Oscillation and solar cycles which may manifest as variations in the latitudinal position of the Intertropical Convergence Zone (ITCZ) which impact Northern Hemisphere temperatures and wind intensity.

Acknowledgments
Geochemical data ($\delta^{15}N_{sed}$, wt % C_{org}, and wt % bSi) used in this study is available in supporting information. This work was supported by a National Science Foundation grant (OCE-0727123 to W.B.). We would like to acknowledge that this work was supported and critiqued by Donn Gorsline who served on Caitlin Tems' PhD dissertation committee but was not able to see this work come to fruition. Additionally, we would like to thank Alexander van Geen, Nick Rollins, Jennifer Lehman, John Fleming, Amy Townsend-Small, Maria Prokopenko, James McManus, Curtis Deutsch, Gerald Haug, Doug Capone, Frank Corsetti, UC Davis Stable Isotope Facility, and Captain and Crew of the RV *Horizon*.

References

Agnihotri, R., M. A. Altabet, T. D. Herbert, and J. E. Tierney (2008), Subdecadally resolved paleoceaongraphy of the Peru margin during the last two millennia, *Geochem., Geophys., Geosyst.*, *9*, Q05013, doi:10.1029/2007GC001744.

Altabet, M. A., and R. Francois (1994), Sedimentary nitrogen isotopic ratio as a recorder for surface ocean nitrate utilization, *Global Biogeochem. Cycles*, *8*, 103–116, doi:10.1029/93GB03396.

Altabet, M. A., R. Francois, D. W. Murray, and W. L. Prell (1995), Climate-related variations in denitrification in the Arabian Sea from sediment $^{15}N/^{14}N$ ratios, *Nature*, *373*(6514), 506–509, doi:10.1038/373506a0.

Altabet, M. A., C. Pilskaln, R. Thunell, C. Pride, D. Sigman, F. Chavez, and R. Francois (1999), The nitrogen isotope biogeochemistry of sinking particles from the margin of the eastern North Pacific, *Deep Sea Res., Part I*, *46*, 655–679, doi:10.1016/S0967-0637(98)00084-3.

Anderson, R. Y. (1992), Possible connection between surface wind activity and the Earth's magnetic field, *Nature*, *358*, 51–53.

Babbin, A. R., R. G. Keil, A. H. Devol, and B. B. Ward (2014), Organic matter stoichiometry, flux, and oxygen control nitrogen loss in the ocean, *Science*, *344*, 406–408, doi:10.1126/science.1248364.

Barron, J. A., Bukry, D., and J. L. Bishchoff (2003), A 2000-yr-long record of climate from the Gulf of California, in *Proceedings of the 19th PACLIM Workshop, Technical Report 71 of the Interagency Ecological Program for the San Francisco Estuary*, edited by G. J. West and N. L. Blomquist, pp. 11–21, Asilomar, Calif.

Barron, J. A., and D. Bukry (2007), Solar forcing of Gulf of California climate during the past 2000 yr suggested by diatoms and silicoflagellates, *Mar. Micropaleontol.*, *62*, 115–139.

Baumgartner, T. R., A. Soutar, and V. Ferreira-Bartrina (1992), Re-construction of the history of Pacific sardine and northern anchovy populations over the past two millennia from sediments of the Santa Barbara basin, California, *CalCOFI Rep.*, *33*, 24–40.

Benton, M. J., and R. J. Twitchett (2003), How to kill (almost all life: The end-Permian extinction event, *Trends Ecol. Evol.*, *18*(7), 358–365, doi:10.1016/S0169-5347(03)00093-4.

Bloemendal, J., B. Lamb, and J. King (1988), Paleoenvironmental implications of rock-magnetic properties of late Quaternary sediment cores from the eastern equatorial Atlantic, *Paleoceanography*, *3*, 61–87, doi:10.1029/PA003i001p00061.

Bograd, S. J., C. G. Castro, E. Di Lorenzo, D. M. Palacios, H. Hailey, W. Gilly, and F. P. Chavez (2008), Oxygen declines and the shoaling of the hypoxic boundary in the California Current, *Geophys. Res. Lett.*, *35*, L12607, doi:10.1029/2008GL034185.

Burroughs, W. J. (1992), *Weather Cycles: Real or Imaginary?* pp. 201, Cambridge Univ. Press, New York.

Chazen, C. R., M. A. Altabet, and T. D. Herbert (2009), Abrupt mid-Holocene onset of centennial-scale climate variability on the Peru-Chile Margin, *Geophys. Res. Lett.*, *36*, L18704, doi:10.1029/2009GL039749.

Chong, L. S., M. G. Prokopenko, W. M. Berelson, A. Townsend-Small, and J. McManus (2012), Nitrogen cycling within suboxic and anoxic sediments from the continental margin of western North America, *Mar. Chem.*, *128–129*, 13–25, doi:10.1016/j.marchem.2011.10.007.

Collins, C. A., N. Garfield, A. S. Mascarenhas, M. G. Spearman, and T. A. Rago (1997), Ocean currents across the entrance to the Gulf of California, *J. Geophys. Res.*, *102*(C9), 20,927–20,936.

DeMaster, D. J. (1979), *The Marine Budgets of Silica and ^{32}Si*, Yale Univ., New Haven.

DeMaster, D. J. (1991), *Measuring Biogenic Silica in Sediments and Suspended Matter*, AGU, Washington, D. C.

Deutsch, C., D. M. Sigman, R. C. Thunell, A. Nele Meckler, and G. H. Haug (2004), Isotopic constraints on glacial/interglacial changes in the oceanic nitrogen budget, *Global Biogeochem. Cycles*, *18*, doi:10.1029/2003GB002189.

Deutsch, C., et al. (2014), Centennial changes in North Pacific anoxia linked to tropical trade winds, *Science*, *345*(6197), 665–668, doi:10.1126/science.1252332.

Douglas, R., O. Gonzalez-Yajimovich, J. Ledesma-Vazquez, and F. Staines-Urias (2007), Climate forcing, primary production and the distribution of Holocene biogenic sediments in the Gulf of California, *Quat. Sci. Rev.*, *26*, 115–129, doi:10.1016/j.quascirev.2006.05.003.

Feely, R. A., C. L. Sabine, J. M. Hernandez-Ayon, D. Ianson, and B. Hales (2008), Evidence for upwelling of corrosive "acidified" water onto the continental shelf, *Science*, *320*, 1490–1492.

Fernández-Barajas, M. E., M. A. Monreal-Gómez, and A. Molina-Cruz (1994), Thermohaline structure and geostrophic flow in the Gulf of California, during 1992, *Ciencias Marinas*, *20*, 267–286.

Ganeshram, R. S., T. F. Pedersen, S. E. Calvert, and J. W. Murray (1995), Large changes in oceanic nutrient inventories from glacial to interglacial periods, *Nature*, *376*, 755–758.

Ganeshram, R. S., T. F. Pedersen, S. E. Calvert, G. W. McNeil, and M. R. Fontugne (2000), Glacial-interglacial variability in denitrification in the world's oceans: Causes and consequences, *Paleoceanography*, *15*(4), 361–376, doi:10.1029/1999PA000422.

Gilly, W. F., J. M. Beman, S. Y. Litvin, and B. H. Robinson (2013), Oceanographic and biological effects of shoaling of the oxygen minimum zone, *Annu. Rev. Mar. Sci.*, *5*, 21.1–21.28, doi:10.1146/annurev-marine-120710-100849.

González-Yajimovich, O., R. G. Douglas, and D. S. Gorsline (2005), The preserved carbonate record in Holocene sediments of the Alfonso and Pescadero basins, Gulf of California, Mexico, *Proc. Geol. Assoc.*, *116*, 315–330.

Gutiérrez, D., et al. (2009), Rapid reorganization in ocean biogenochemistry off Peru towards the end of the Little Ice Age, *Biogeosciences*, *6*, 835–848.

Hendy, I. L., T. J. Napier, and A. Schimmelmann (2015), From extreme rainfall to drought: 250 years of annually resolved sediment deposition in Santa Barbara Basin, California, *Quat. Int.*, *387*, 3–12.

Jones, C. E., and H. C. Jenkyns (2001), Seawater strontium isotopes, ocean anoxic events, and seafloor hydrothermal activity in the Jurassic and Cretaceous, *Am. J. Sci.*, *301*, 112–149.
Keeling, R. F., A. Körtzinger, and N. Gruber (2010), Ocean deoxygenation in a warming world, *Annu. Rev. Mar. Sci.*, *2*, 199–229, doi:10.1146/annurev.marine.010908.163855.
Khider, D., C. S. Jackson, and L. D. Stott (2014), Assessing millennial-scale variability during the Holocene: A perspective from the western tropical Pacific, *Paleoceanography*, *29*, 143–159, doi:10.1002/2013PA002534.
King, J. W., and J. E. T. Channell (1991), Sedimentary magnetism, environmental magnetism, and magnetostratigraphy, Rev. Geophys., suppl., U.S. Natl. Rep. IUGG, 358–370.
Lavín, M. F., and S. G. Marinone (2003), An overview of the physical oceanography of the Gulf of California, in *Nonlinear Processes in Geophysical Fluid Dynamics*, edited by O. U. Velasco Fuentes, pp. 173–204, Kluwer Acad., Netherlands.
Lehmann, M. F., S. M. Bernasconi, A. Barbiere, and J. A. McKenzie (2002), Preservation of organic matter and alteration of its carbon and nitrogen isotope composition during simulated and in situ early sedimentary diagenesis, *Geochim. Cosmochim. Acta*, *66*(20), 3573–3582, doi:10.1016/S0016-7037(02)00968-7.
Liu, Z., M. A. Altabet, and T. D. Herbert (2008), Plio-Pleistocene denitrification in the eastern tropical North Pacific: Intensification at 2.1 Ma, *Geochem., Geophys., Geosyst.*, *9*, Q11006, doi:10.1029/2008GC002044.
Lomb, N. R. (1976), Least-squares frequency analysis of unequally spaced data, *Astrophys. Space Sci.*, *39*, 447–462.
MacDonald, G. M., and R. A. Case (2005), Variations in the Pacific Decadal Oscillation over the past millennium, *Geophys. Res. Lett.*, *32*, L08703, doi:10.1029/2005GL022478.
Mantua, N. J., and S. R. Hare (2002), The Pacific Decadal Oscillation, *J. Oceanogr.*, *58*, 35–44, doi:10.1023/A:1015820616384.
McClatchie, S., R. Goericke, R. Cosgrove, G. Auad, and R. Vetter (2010), Oxygen in the Southern California Bight: Multidecadal trends and implications for demersal fisheries, *Geophys. Res. Lett.*, *37*, L19602, doi:10.1029/2010GL044497.
Minobe, S. (1997), A 50–70 year climatic oscillation over the North Pacific and North America, *Geophys. Res. Lett.*, *24*, 683–686, doi:10.1029/97GL00504.
Meko, D. M. (1992), Spectral properties of tree-ring data in the United States Southwest as related to El Niño/Southern Oscillation, in *El Niño: Historical and Paleoclimatic Aspects of the Southern Oscillation*, edited by H. F. Diaz and V. Markgraf, pp. 227–242, Cambridge Univ. Press, New York.
Ogurtsov, M. G., Y. A. Nagovitsyn, G. E. Kocharov, and H. Junger (2002), Long-period cycles of the Sun's activity recorded in direct solar data and proxies, *Sol. Phys.*, *211*, 371–394.
Olsson, I. (1986), Radiometric methods, in *Handbook of Holocene Palaeoecology and Palaeohydrology*, edited by B. Berglund, pp. 273–312, John Wiley, Chichester.
Pérez-Cruz, L. (2013), Hydrological changes and paleoproductivity in the Gulf of California during the middle and late Holocene and their relationship with ITCZ and North American Monsoon variability, *Quat. Res.*, *79*, 138–151.
Pichevin, L., R. S. Ganeshram, B. C. Reynolds, F. Prahl, T. F. Pederson, R. Thunell, and E. L. McClymont (2012), Silicic acid biogeochemistry in the Gulf of California: Insights from sedimentary Si isotopes, *Paleooceanography*, *27*, PA2201, doi:10.1029/2011PA002237.
Pierce, S. D., J. A. Barth, R. K. Shearman, and A. Y. Erofeev (2012), Declining oxygen in the northeast Pacific, *J. Phys. Oceanogr.*, *42*(3), 495–501, doi:10.1175/JPO-D-11-0170.1.
Pike, J., and A. E. S. Kemp (1997), Early Holocene decadal-scale ocean variability recorded in Gulf of California laminated sediments, *Paleoceanography*, *12*(2), 227–238, doi:10.1029/96PA03132.
Poore, R. Z., T. M. Quinn, and S. Verardo (2004), Century-scale movement of the Atlantic Intertropical Convergence Zone linked to solar variability, *Geophys. Res. Lett.*, *31*, L12214, doi:10.1029/2004GL019940.
Price, N. B., and S. E. Calvert (1977), Contrasting geochemical behaviors of iodine and bromine in recent sediments from Namibian Shelf, *Geochim. Cosmochim. Acta*, *41*, 1769–1775.
Pride, C., R. Thunell, D. Sigman, L. Keigwin, M. Altabet, and E. Tappa (1999), Nitrogen isotopic variations in the Gulf of California since the Last Deglaciation: Response to global climate change, *Paleococeanography*, *14*(3), 397–409, doi:10.1029/1999PA900004.
Prokopenko, M., D. E. Hammond, A. J. Spivack, and L. Stott (2006), Impact of long-term diagenesis on δ^{15}N of organic matter in marine sediments: Sites 1227 and 1230, *Proc. Ocean Drill. Program, Sci. Results*, *201*, 30.
Prokopenko, M., D. M. Sigman, W. M. Berelson, D. E. Hammond, B. Barnett, L. Chong, and A. Townsend-Small (2011), Denitrification in anoxic sediments supported by biological nitrate transport, *Geochim. Cosmochim. Acta*, *75*, 7180–7199, doi:10.1016/j.gca.2011.09.023.
Ragueneau, O., et al. (2000), A review of the Si cycle in the modern ocean: Recent progress and missing gaps in the application of biogenic opal as a paleoproductivity proxy, *Global Planet. Change*, *26*, 317–365, doi:10.1016/S0921-8181(00)00052-7.
Reimer, P. J., et al. (2013), IntCal13 and MARINE13 radiocarbon age calibration curves 0–50000 years cal BP, *Radiocarbon*, *55*(4), doi:10.2458/azu_js_rc.55.16947.
Ricaurte-Villota, C., O. Gonzalez-Yajimovich, and A. Sanchez (2013), Coupled response of rainfall and denitrification to solar forcing during the Holocene in Alfonso Basin, *Ciencias Marinas*, *39*(2), 151–164.
Riser, S. C., and K. S. Johnson (2008), Net production of oxygen in the subtropical ocean, *Nature*, *451*(7176), 323–325, doi:10.1038/nature06441.
Scargle, J. D. (1982), Studies in astronomical time series analysis. II—Statistical aspects of spectral analysis of unevenly spaced data, *Astrophys. J.*, *263*(2), 835–853.
Scargle, J. D. (1989), Studies in astronomical time series analysis. III—Fourier transforms, autocorrelation functions, and cross-correlation functions of unevenly spaced data, *Astrophys. J.*, *343*(2), 874–887.
Schlesinger, M. E., and N. Ramankutty (1994), An oscillation in the global climate system of period 65–70 years, *Nature*, *3*(67), 723–726.
Schulz, M., and M. Mudelsee (2002), REDFIT: Estimating red-noise spectra directly from unevenly spaced paleoclimatic time series, *Comput. Geosci.*, *28*, 421–426.
Schulz, M., and K. Stattegger (1997), SPECTRUM: Spectral analysis of unevenly spaced time series, *Comput. Geosci.*, *23*(9), 929–945.
Sharp, G. D. (1992), Fishery catch records, El Niño/Southern Oscillation, and longer-term climate change as inferred from fish remains in marine sediments, in *El Niño: Historical and Paleoclimatic Aspects of the Southern Oscillation*, edited by H. F. Diaz and V. Markgraf, pp. 379–418, Cambridge Univ. Press, New York.
Sigman, D. M., J. Granger, P. J. Difiore, M. M. Lehmann, R. Ho, G. Cane, and A. Van Geen (2005), Coupled nitrogen and oxygen isotope measurements of nitrate along the eastern North Pacific margin, *Global Biogeochem. Cycles*, *19*, GB4022, doi:10.1029/2005GB002458.
Southon, J. R., and G. M. Santos (2004), Ion source development at KCC AMS, University of California, Irvine, *Radiocarbon*, *46*, 33–39.
Southon, J. R., and G. M. Santos (2007), Life with MC-SNICS. Part II: Further ion source development at the Keck carbon cycle AMS facility, *Nucl. Instrum. Methods Phys. Res., Sect. B*, *259*, 88–93.

Staines-Urías, F., R. G. Douglas, and D. S. Gorsline (2009), Oceanographic variability in the southern Gulf of California over the past 400 years: Evidence from faunal and isotopic records from planktic foraminifera, *Palaeogeography, Palaeoclimatology, Palaeoecology*, *284*(3–4), 337–354, doi:10.1016/j.palaeo.2009.10.016.

Stramma, L., G. C. Johnson, J. Sprintall, and V. Mohrholz (2008), Expanding oxygen-minimum zones in the tropical oceans, *Science*, *320*, 655–658.

Strickland, J. P. T. (1968), A practical handbook of seawater analysis, Fisheries Research Board of Canada, Halifax.

Stuiver, M., and A. H. Polach (1977), Discussion: Reporting of ^{14}C data, *Radiocarbon*, *19*, 355–363.

Stuiver, M., and P. J. Reimer (1993), Extended ^{14}C database and revised CALIB radiocarbon calibration program, *Radiocarbon*, *35*, 215–230.

Tems, C. E., W. M. Berelson, and M. G. Prokopenko (2015), Particulate $\delta^{15}N$ in laminated marine sediments as a proxy for mixing between the California Undercurrent and the California Current: A proof of concept, *Geophys. Res. Lett.*, *42*, 419–427, doi:10.1002/2014GL061993.

Thunell, R. C., C. J. Pride, E. Tappa, and F. E. Muller-Karger (1994), Biogenic silica fluxes and accumulation rates in the Gulf of California, *Geology*, *22*, 303–306, doi:10.1130/0091-7613(1994)022<0303:BSFAAR>2.3.CO;2.

Thunell, R. C., and A. B. Kepple (2004), Glacial-Holocene $\delta^{15}N$ record from the Gulf of Tehuantepec, Mexico: Implications for denitrification in the eastern equatorial Pacific and changes in atmospheric N_2O, *Global Biogeochem. Cycles*, *18*, GB1001, doi:10.1029/2002GB002028.

Thunell, R., D. M. Sigman, F. E. Muller-Karger, Y. Astor, and R. Varela (2004), Nitrogen isotopic dynamics of the Cariaco Basin, Venezuela, *Global Biogeochem. Cycles*, *18*, GB3001, doi:10.1029/2003GB002185.

Thurow, J., and M. Schaaf (1995), A comparison of Holocene to late Pleistocene grayvalue-time-series of sediments from the Santa Barbara Basin (ODP Site 893) and the Guaymas Basin (DSDP Site 480), in IGCP 374: Palaeoclimatology and Palaeoceanography From Laminated Sediments, edited by R. J. Behl and J.P. Kennett, 33 pp.

Townsend-Small, A., M. G. Prokopenko, and W. M. Berelson (2014), Nitrous oxide cycling in the water column and sediments of the oxygen minimum zone, eastern subtropical North Pacific, Southern California, and Northern Mexico (23°N–34°N), *J. Geophys. Res. Oceans*, *119*, 3158–3170, doi:10.1002/2013JC009580.

Welch, P. D. (1967), The use of fast Fourier transform for the estimation of power spectra: A method based on time averaging over short, modified periodograms, *IEEE Trans. Audio Electroacoust.*, *15*(2), 70–73.

Ward, B. B., C. B. Tuit, J. Am, J. J. Rich, J. Moffett, S. Wajih, and A. Naqvi (2008), Organic carbon, not copper, controls denitrification in oxygen minimum zones of the ocean, *Deep Sea Res., Part I*, *55*, 1672–1683.

Ward, B. B., A. H. Devol, J. J. Rich, B. X. Chang, S. E. Bulow, H. Naik, A. Pratihary, and A. Jayakumar (2009), Denitrification as the dominant nitrogen loss process in the Arabian Sea, *Nature*, *461*, 78–82, doi:10.1038/nature08276.

White, A. E., R. A. Foster, C. R. Benitez-Nelson, P. Masqué, E. Verdeny, B. N. Popp, K. E. Arthur, and F. G. Prahl (2013), Nitrogen fixation in the Gulf of California and the Eastern Tropical North Pacific, *Prog. Oceanogr.*, *109*, 1–17, doi:10.1016/j.pocean2012.09.002.

Wingall, P. B., and R. J. Twitchett (1996), Ocean anoxia and the end Permian mass extinction, *Science*, *272*(5265), 1155–1158, doi:10.1126/science.272.5265.1155.

Xu, X., S. E. Trumbore, S. H. Zheng, J. R. Southon, K. E. McDuffee, M. Luttgen, and J. C. Liu (2007), Modifying a sealed tube zinc reduction method for preparation of AMS graphite targets: Reducing background and attaining high precision, *Nucl. Instrum. Methods Phys. Res., Sect. B*, *259*, 320–329.

Ziegler, M., T. Jilbert, G. J. de Lange, L. J. Lourens, and G.-J. Reichart (2008), Bromine counts from XRF scanning as an estimate of the marine organic carbon content of sediment cores, *Geochem., Geophys., Geosyst.*, *9*, Q05009, doi:10.1029/2007GC001932.